Exploring the effect of geometric coupling on friction and energy dissipation in rough contacts of elastic and viscoelastic coatings

N. Menga,[1, 2, *] G. Carbone,[1, 2] and D. Dini[2]

[1]*Department of Mechanics, Mathematics and Management,*
Politecnico of Bari, V.le Japigia, 182, 70126, Bari, Italy
[2]*Imperial College London, Department of Mechanical Engineering,*
Exhibition Road, London SW7 2AZ

Abstract

We study the frictional behavior of both elastic and viscoelastic thin coatings bonded to a seemingly rigid substrate and sliding against a rough profile in the presence of Coulomb friction at the interface. The aim is to explore the effect of the coupling between the normal and tangential displacement fields arising from the finiteness of the material thickness and to quantify the contribution this can have on energy losses.

We found that, due to normal-tangential coupling, asymmetric contacts and consequently additional friction are observed even for purely elastic layers, indeed associated with zero bulk energy dissipation. Furthermore, enhanced viscoelastic friction is reported in the case of viscoelastic coatings due to coupling, this time also entailing larger bulk energy dissipation.

Geometric coupling also introduces additional interactions involving the larger scales normal displacements, which leads to a significant increase of the contact area, under given normal load, compared to the uncoupled contacts.

These results show that, in the case of contact interfaces involving thin deformable coating bonded to significantly stiffer substrate, the effect of interfacial shear stresses on the frictional and contact behavior cannot be neglected.

---

*Electronic address: nicola.menga@poliba.it

I. INTRODUCTION

Nowadays, a large number of systems in several application fields involve thin solid films. Soft coatings are one of the most frequent examples of such cases: a thin layer of compliant material with specific characteristics is deposited onto a significantly stiffer substrate (thus considered as rigid) in order to tailor the overall system behavior (e.g. chemical resistance to corrosion, enhanced or reduced stiffness, damping, frictional behavior). Possible applications range from engines, where specific low friction coatings are adopted to reduce energy dissipation in key contacting pairs (e.g. valve train systems and crankshafts [1, 2]), to robotic clamps for objects manipulation [3] or anti-skid tapes for ramps and stairs, where high frictional coatings are instead required to increase the grip. Coatings are also present in the case of biological systems such as human hands and feet, where the covering skin (which may locally be constituted by very thin layers) concurs in developing the high interfacial friction sustaining, for instance, the firm hand grip on the tennis racket handle, or the barefoot walking on different grounds.

For these reasons, a constantly rising interest on the tribological behavior of solid thin films, often studied as compliant layers of materials bonded to rigid bodies and indented by other rigid or deformable rough contersurfaces, has been reported in the last decades. Indeed, besides the theoretical [4–11], numerical [12–17] and experimental [18–21] studies focusing on contact problems of semi-infinite bodies, detailed investigations have been also devoted to the case of contacts involving thin bodies [22–27, 44].

To this regard, it is well known that dealing with half-space contacts, a certain degree of coupling between the normal and tangential displacement fields occurs in the case of material dissimilarity [32, 33]. Such a *material* coupling is governed by the Dundurs' second constant, often referred to as β, which if one of the bodies is rigid takes the value $\beta = (1 - 2\nu)/2(1 - \nu)$, with ν being the Poisson's ratio. This effect has been explored in several studies, mostly focusing on stick-slip fretting problems associated to homogeneous [34–36] and graded [37, 38] elastic materials. Interestingly, in [34] it was reported that, in the case of dissimilar cylinders contacts, a non-negligible influence of the material coupling occurs on both the normal stiffness of the contact and the contact pressure distribution. However, a few pioneeristic studies [29–31], dealing with thin deformable layers, have shown that such a simple coupling representation is no longer valid as, since the normal deformation cannot be accommodated remotely as in the case of half-space, two possible independent sources of normal-tangential interactions exist: (i) the *material* coupling, due to material dissimilarity, governed by the Dundurs' second constant β; and (ii) an additional *geometric* (or domain shape) coupling, which depends on the layer thickness (i.e. it vanishes for thick layers) and still occurs even in the case of similar contact pairs (i.e. $\beta = 0$). Significantly less effort has been made to investigate the effect of the latter on the contact behavior of thin films. Indeed, moving from the pioneeristic study of Bentall and Johnson [29], only a few authors have approached the problem [30, 31, 39, 40] focusing on smooth single asperity contacts and showing a significant contact pressure asymmetry arising from the coupling. Furthermore, in a recent study [28], the rough contact behavior of elastic thin layers in the presence of interfacial friction has been investigated, showing that, even in the case of $\beta = 0$, the *geometric* coupling between the normal and tangential elastic fields may lead to a significant increase of the effective contact area, with non-negligible implication on contact-related phenomena such as interfacial hydraulic impedance, electrical conductivity [41], and wear process evolution [42]. Interestingly, the *geometric* coupling may play an

even more dramatic role in determining the frictional performance of interfaces in relative motion due to the asymmetry of the contact pressure distribution observed in Refs. [28, 30, 31]. Focusing, for instance, on viscoelastic contact of thin layers, one can reasonably expect different energy dissipation due to bulk viscoelasticity and, in turn different frictional behavior of the interface, depending on the specific *geometric* coupling effect on the contact pressure and contact spots distribution which alter the effective excitation spectra during sliding. To the best of the authors knowledge, an investigation on this effect is currently missing in the specialized literature, and this work aims at filling this gap.

In this study we focus on the case of a thin coating, sufficiently softer than the underlying substrate so that the latter can be assumed as rigid, in frictional sliding contact with a rigid profile with self-affine roughness. We consider both elastic and viscoelastic coating materials. We investigate in details the effect of normal-tangential coupling in thin films on both the overall contact behavior and frictional response of the system, with further focus on the energy dissipation. As already mentioned, the system configuration studied here covers several technological applications related to the grip performance of bio-inspired or natural system for handling of objects as well as many other interesting problems, including protein-coated interfaces, paints and soft coatings for industrial use, finger tip contact with touch screens.

II.   THE CONTACT PROBLEM FORMULATION

The system under investigation is shown in Figure 1, where a thin soft coating bonded to a rigid substrate is sketched. The free surface of the coating layer is indented by a rigid profile with roughness $r(x)$. According to Fig. 1, we define h the coating thickness, λ the roughness fundamental wavelength, and V the profile sliding speed. In our formulation, we assume $V \ll c_s$ with c_s being the sound speed into the coating material; furthermore, we focus on long time observations so that steady state conditions can be reasonably assumed. In what follows, we will adopt subscript 1 and 2 referring to tangential and normal quantities, respectively. Indeed, in Fig. 1, δ_2 is the total normal displacements of the rough profile, $\bar{u}_2$ is the mean normal displacement of the coating surface, whereas Δ is the mean penetration of the rigid profile into the deformable coating. Note that $\delta_2 = \Delta + \bar{u}_2$.

The presence of Amonton/Coulomb friction is taken into account at the contact interface. This means that, given a generic normal contact pressure distribution $p(x)$, a corresponding tangential shear stress distribution also acts on the contacting parts in the form

$$\tau(x) = \mu_c p(x); \qquad x \in \Omega, \tag{1}$$

where μ_c is the friction coefficient, and $\Omega = U_{i=1}^{L}[\alpha_i, \beta_i]$ is the contact domain, being α_i and β_i the unknown coordinates of i-th contact spot, with $\alpha_i < \beta_i$ and $i = 1, 2, ..., L$, where L is the unknown number of contacts. Notably, we assume μ_c independent of the relative sliding speed.

The contact problem approach exploits the reliable formulation developed in Refs [43, 44]. Indeed, building on the linearity of the material response and exploiting the problem translational invariance, the interfacial layer displacement vector $\mathbf{v} = (v_1, v_2)$ can be linked to the stress vector $\sigma = (\mu_c p, -p)$ by means of

$$\mathbf{v}(x) = \mathbf{u}(x) - \bar{\mathbf{u}} = \int_{\Omega} ds \Theta(x-s) \sigma(s); \qquad x \in \Omega, \tag{2}$$
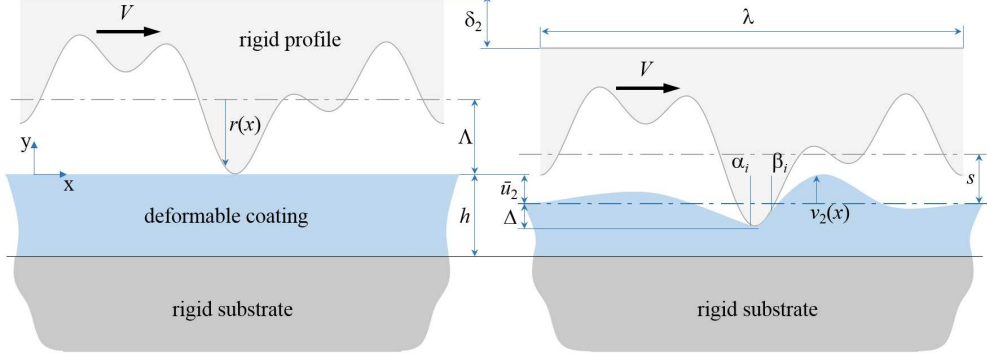
3

FIG. 1: A soft coating of thickness h backed onto a rigid substrate is in sliding contact with a rigid rough profile. Coulomb friction interactions occur at the interface. The contact mean penetration is indicated with Δ, the profile peak height is Λ, and the roughness fundamental wavelength is λ.

where the time-dependency of the stress and deformation fields has been removed by invoking the coordinate transformation $x - Vt \to x$.

In Eq. (2), $\mathbf{u}$ is the total displacement vector, and $\bar{\mathbf{u}}$ is the mean displacement vector given by

$$\bar{u}_1 = q_0 h \frac{1+\nu}{\pi E_0} \tau_{\mathrm{m}} \lambda, \tag{3}$$

$$\bar{u}_2 = q_0 h \frac{1-2\nu}{2\pi E_0} p_{\mathrm{m}} \lambda, \tag{4}$$

where $q_0 = 2\pi/\lambda$ and E_0 is zero-frequency elastic modulus. Notably, $p_m = \frac{1}{\lambda} \int_\Omega p(x)\, dx$ and $\tau_m = \frac{1}{\lambda} \int_\Omega \tau(x)\, dx$ are the mean contact pressure and shear stress, respectively.

The term $\Theta(x) = \Theta_{kl}(x)$, with $k, l = 1, 2$ is the Green's tensor which takes different forms depending on whether the coating is elastic or viscoelastic. Indeed, in the elastic case, we have

$$\Theta_{kl}(x) = \frac{G_{kl}(x)}{E_0}, \tag{5}$$

with $G_{kl}(x)$ given by Ref. [28] as

$$G_{11}(x) = -\frac{2(1-\nu^2)}{\pi} \left[\log \left| 2 \sin \left(\frac{q_0 x}{2} \right) \right| + \sum_{m=1}^{\infty} B(mq_0 h) \frac{\cos(mq_0 x)}{m} \right], \tag{6}$$

$$G_{12}(x) = -G_{21}(x) = \frac{1+\nu}{\pi} \left[\frac{1-2\nu}{2} \left[\operatorname{sgn}(x)\pi - q_0 x \right] - \sum_{m=1}^{\infty} C(mq_0 h) \frac{\sin(mq_0 x)}{m} \right], \tag{7}$$

$$G_{22}(x) = -\frac{2(1-\nu^2)}{\pi} \left[\log \left| 2 \sin \left(\frac{q_0 x}{2} \right) \right| + \sum_{m=1}^{\infty} A(mq_0 h) \frac{\cos(mq_0 x)}{m} \right], \tag{8}$$

with

$$A\left(mq_0h\right) = 1 + \frac{2mq_0h - (3 - 4\nu)\sinh\left(2mq_0h\right)}{5 + 2\left(mq_0h\right)^2 - 4\nu\left(3 - 2\nu\right) + (3 - 4\nu)\cosh\left(2mq_0h\right)}, \tag{9}$$

$$B\left(mq_0h\right) = 1 - \frac{2mq_0h + (3 - 4\nu)\sinh\left(2mq_0h\right)}{5 + 2\left(mq_0h\right)^2 - 4\nu\left(3 - 2\nu\right) + (3 - 4\nu)\cosh\left(2mq_0h\right)}, \tag{10}$$

$$C\left(mq_0h\right) = \frac{4\left(1 - \nu\right)\left[2 + \left(mq_0h\right)^2 - 6\nu + 4\nu^2\right]}{5 + 2\left(mq_0h\right)^2 - 4\nu\left(3 - 2\nu\right) + (3 - 4\nu)\cosh\left(2mq_0h\right)}. \tag{11}$$

On the other hand, in the case of viscoelastic coatings, extending the formulation given in Refs. [25, 44], the Green's tensor takes the form

$$\Theta_{kl}^V\left(x\right) = J\left(0^+\right)G_{kl}\left(x\right) + \int_{0^+}^{+\infty} G_{kl}\left(x + Vt\right)\dot{J}\left(t\right)dt, \tag{12}$$

which, this time, in order to take into account for the response delay in the viscoelastic material, parametrically depends on the sliding speed. In Eq. (12), the tern $J\left(t\right)$ is the viscoelastic creep function, which for a linear viscoelastic material with one relaxation time τ takes the form

$$J\left(t\right) = H\left(t\right)\left[\frac{1}{E_0} - \frac{1}{E_1}\exp\left(-t/\tau\right)\right], \tag{13}$$

where $H\left(t\right)$ is the Heavyside step function, and $1/E_1 = 1/E_0 - 1/E_\infty$, with E_∞ being the high-frequency elastic modulus.

Regardless of the coating material rheology, the solution of the contact problem is found by observing that, within the contact domain Ω, the normal interfacial displacement must match the rough profile shape $r\left(x\right)$. Referring to Fig. 1, from the normal projection of Eq. (2) we have

$$\Lambda - r\left(x\right) - \Delta = \int_\Omega ds\left[\mu_c\Theta_{21}\left(x - s\right) - \Theta_{22}\left(x - s\right)\right]p\left(s\right); \qquad x \in \Omega, \tag{14}$$

where the only unknowns are the pressure distribution $p\left(x\right)$ and the coordinates α_i, β_i corresponding to the individual contact edges. By relying on the numerical strategy based on a non-uniform contact area discretization developed in Ref. [43], for any given value of the contact penetration Δ, Eq. (14) can be numerically solved for $p\left(x\right)$, once fixed α_i, β_i. Further, the exact size of the contact area can be calculated, iteratively, by observing that, dealing with adhesiveless contact conditions, bounded contact stress are prescribed, specifically vanishing at the contact edges. Indeed, referring to Refs. [25, 44, 45] we have that

$$K_{I,\alpha_i} = -\lim_{x\to\alpha_i^+}\sqrt{2\pi\left(x - \alpha_i\right)}p\left(x\right) = 0, \tag{15}$$

$$K_{I,\beta_i} = -\lim_{x\to\beta_i^-}\sqrt{2\pi\left(\beta_i - x\right)}p\left(x\right) = 0, \tag{16}$$

where K_I is the mode I stress intensity factor.

III. RESULTS AND DISCUSSION

The presence of a deformable layer of finite thickness gives rise to coupling between the normal and tangential displacement fields [32, 33]. Indeed, in agreement with [28, 29], focusing on the cross-coupled Green's function G_{12} given in Eq. (7), we observe two coupling terms: the first right-hand side term represents the *material* coupling, taking into account for the normal-tangential interactions in contact pairs of dissimilar materials. Notably, by recalling the Dundurs' second constant expression assuming one of the contacting bodies as rigid $\beta = (1 - 2\nu)/2(1 - \nu)$, we observe that material coupling vanishes for $\beta = 0$ [32–34]. The second right-hand side term in Eq. (7) is an additional source of normal-tangential coupling, this time called *geometric*, which is a function of the layer size through the thickness h, and is non-vanishing even for $\beta = 0$. Notably, in the limit of semi-infinite bodies (i.e. for $h \to \infty$) the latter term vanishes, thus leading to the well-known half-plane or half-space behavior for which normal-tangential coupling only depends on the value of β [32, 33].

In what follows, we focus on the case of $\beta = 0$ (i.e. $\nu = 0.5$) so that the whole normal-tangential coupling arises from the finiteness of the layer thickness h (the case with $\beta \neq 0$ is briefly discussed in Appendix). We aim at investigate the frictional behavior of both elastic and viscoelastic interfaces in coupled conditions, with specific focus on the interfacial and bulk energy dissipation. Furthermore, the contact behavior of purely viscoelastic rubber-like coatings is also investigated in terms of mean contact quantities (i.e. contact area size, contact mean pressure and penetration, displacement field). In order to highlight the specific effect of geometric normal-tangential coupling on the investigated quantities we compare the results against those related to frictionless conditions (i.e. $\mu_c = 0$), where no coupling effect occurs[34].

All the calculations have been performed considering a self-affine roughness on the rigid profile. The different profile shapes have been numerically generated by exploiting the technique reported in Ref. [44]. The Power Spectral Density (PSD) $C_r(q) = (2\pi)^{-1} \int dx \, \langle r(0) r(x) \rangle e^{-iqx}$ of the considered roughness is given by

$$C_r(q) = C_0 \left(\frac{|q|}{q_0} \right)^{-(2H+1)} ; \qquad q \in [q_0, q_1]$$

$$C_r(q) = 0; \qquad q \notin [q_0, q_1] \tag{17}$$

where $q_1 = N q_0$ (being N the number of roughness scales) and H is the Hurst exponent, which is related to the fractal dimension by $D_f = 2 - H$. Profiles are generated assuming a root mean square roughness of $r_{rms} = \sqrt{\langle r^2 \rangle} = 10 \ \mu m$, $H = 0.7$, and $N = 100$. Notably, since $q_0 = 2\pi/\lambda$, adjusting the value of λ also modifies the profile average square slope $m_2 = \langle r'^2 \rangle = \int q^2 C_r(q) \, dq$. Moreover, in order to obtain a statistically significant contact behavior, results have been ensemble averaged on several realizations for each value of the contact parameter investigated, and are shown in terms of the following dimensionless quantities: $\tilde{h} = q_0 h$, $\tilde{a} = q_0 a$, $\tilde{\Delta} = \Delta/\Lambda$, $\tilde{v} = v/\Lambda$, $\tilde{\Lambda} = q_0 \Lambda$, $\zeta = V\tau q_0$, and $\tilde{p} = 2(1 - \nu^2) p/(E_0 q_0 \Lambda)$. In viscoelastic calculations we assume $E_\infty/E_0 = 3$.

A. Frictional behavior

In this paper we consider Coulomb friction interactions, which occurs through distributed tangential tractions at the interface, as indicated in Eq. (1). However, in the presence

6

of asymmetric distributions of contact pressure and normal displacement such as those resulting from viscoelastic relaxation delay in sliding contact or normal-tangential anti-symmetric coupling, an additional term on tangential force opposing the motion arises as the tangential component of the normal pressure distribution projected along the local rough profile normal direction. This friction force F_a, induced by asymmetric pressure distribution, is usually calculated as [6, 44]

$$F_a = \int_L p(x) v_2'(x) dx \tag{18}$$

where v_2' is the first spatial derivative of the normal displacement field, and $L = n\lambda$ is the rigid profile length. The corresponding friction coefficient is

$$\mu_a = \frac{F_a}{Lp_m}, \tag{19}$$

so that the total friction force F_t opposing the motion can then be written as

$$F_t = (\mu_c + \mu_a) Lp_m \tag{20}$$

Moreover, since several studies [6, 25] have shown that, under given contact area size, $\mu_a \propto \sqrt{m_2}$, here we normalize friction results by the factor $\sqrt{m_2}$.

1. Elastic contacts

Elastic rough contacts are usually not affected by friction force F_a, as for elastic contacts involving uncoupled half-space (i.e. $h \to \infty$ and $\beta = 0$ so that $G_{12} = 0$) symmetric pressures and displacements are expected. However, when dealing with sufficiently thin films, even for similar contact pairs material (i.e. $\beta = 0$) *geometric* coupling occurs. Since from Eq. (7) the resulting normal-tangential coupling function is an odd function of x, its effect is to introduce a certain degree of asymmetry in the contact pressure and normal displacement distributions. The resulting frictional force F_a opposing the motion can be calculated from Eq. (18) in the Fourier domain as

$$F_a = \frac{\mu_c E_0}{2\pi} \int dq \frac{S_{12}(|q|h)}{S_{22}^2(|q|h) + \mu_c^2 S_{12}^2(|q|h)} q^2 |v_2(q)|^2 \tag{21}$$

where $v_2(q) = \int dx v(x) e^{-iqx}$ is the Fourier transform of the normal displacement field, and $S_{11}(|q|h) = 2(1-\nu^2)[1 - B(qh)]$, $S_{12}(|q|h) = (1+\nu)[C(qh) - (1-2\nu)]$, $S_{22}(|q|h) = 2(1-\nu^2)[1 - A(|q|h)]$. Notably, $F_a = 0$ in the case of both frictionless (i.e. $\mu_c = 0$) or uncoupled (i.e. $h \to \infty$ and $\beta = 0$) contacts.

It is interesting to observe that, since the layer material is purely elastic, such the friction force F_a arising from asymmetric contact pressure distribution does not involve bulk energy dissipation. Indeed, by invoking the energy balance applied to the deformable coating we have that

$$V\left[\int_\Omega p(x) v_2'(x) dx - \mu_c \int_\Omega p(x) v_1'(x) dx\right] = 0 \tag{22}$$

where v_1' is the first spatial derivative of the tangential displacement field.

Figures 2 show the behavior of the friction coefficient μ_a in elastic contacts of thin layers with $\beta = 0$. Specifically, Figure 11a reports the value of the normalized friction coefficient $\mu_a/\sqrt{m_2}$ due to pressure asymmetry as a function of the interfacial Coulomb friction
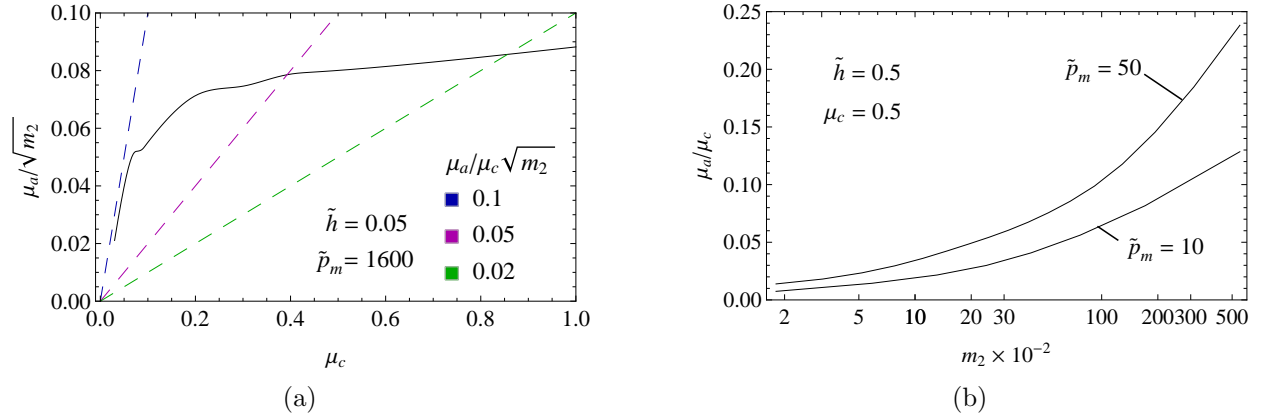
7

FIG. 2: The normalized friction coefficient $\mu_a/\sqrt{m_2}$ due to asymmetric coupled contact pressure as a function of the interfacial Coulomb friction coefficient μ_c (a). The friction ratio μ_a/μ_c as a function of the rigid profile mean square slope m_2 (b). All the data refer to $\beta = 0$, and $m_2 = 0.018$ for (a).

coefficient μ_c for a given layer thickness. We observe that, in agreement with Eq. (21), under load controlled conditions, reducing the tangential stresses (i.e. reducing μ_c) leads to an overall reduction of μ_a. Indeed, the overall normal-tangential coupling is modulated by Coulomb interfacial friction from (see Eq. (2)), therefore reducing μ_c results in a lower degree of asymmetry of the contact pressure distribution, and in turn of μ_a. Moreover, Figure 11a also investigates the friction ratio μ_a/μ_c. This quantity clearly highlight the impact of coupling effect on the overall friction opposing the indenter motion (see Eq. (20)). To this regard, Eq. (21) helps in understanding why reducing μ_c also leads to an increase of μ_a/μ_c as, under load controlled conditions, $\mu_a/\mu_c = F_a/(p_m L \mu_c) \propto 1/(1 + \mu_c^2 c_1)$ with $c_1 > 0$. The friction ratio μ_a/μ_c is also investigated in Figure 11b, this time as a function of the profile mean square slope m_2, showing that, in agreement with Refs [6, 25], increasing m_2 leads to a less than proportional increase of μ_a. Interestingly, assuming m_2 of order unity, as indeed measured for asphalt surfaces [48], a friction coefficient μ_a due to coupling effects as high as $10 \div 20\%$ of μ_c is predicted, thus resulting in a non-negligible coupling effect on the overall friction force opposing the motion.

2. Viscoelastic friction

The physical picture drawn above for elastic materials is still valid in the case of viscoelastic thin coatings. However, in the presence of viscoelasticity a higher degree of contact pressure asymmetry is expected due to delayed material response, which leads to viscous bulk energy dissipation even in the case of semi-infinite uncoupled contacts. As in the previous case section, since we focus on coupling arising from the finite thickness of the viscoelastic layers involved in the contact, with referernce to the scheme reported in Figure 1, we assume $\beta = 0$.

Global effect of coupling on the contact is visualized in figure 3, where the normal displacement field of a thin viscoelastic coating is reported for both coupled (i.e. $\mu_c = 0.8$) and uncoupled (i.e. $\mu_c = 0$). A significant degree of asymmetry between the leading (right-hand
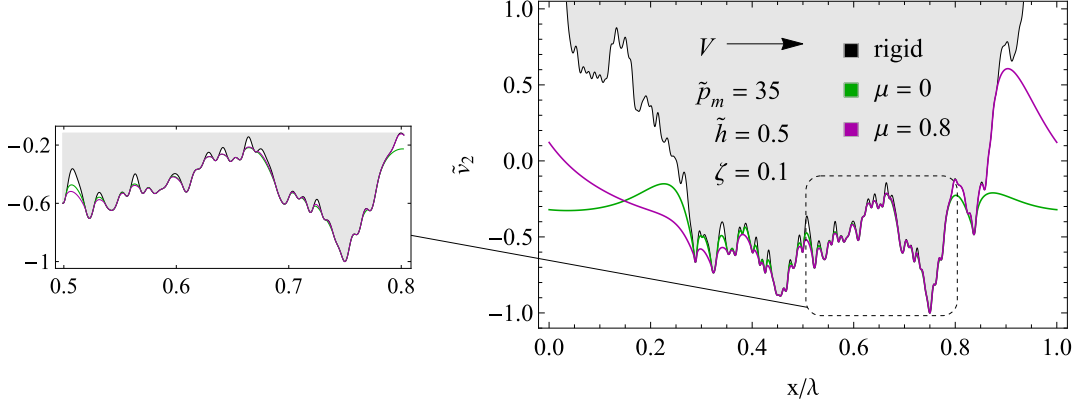
8

FIG. 3: The viscoelastic dimensionless normal displacement $\tilde{v}_2 = (v_2 + \Delta)/\Lambda - 1$, under fixed normal load, in both coupled ($\mu_c = 0.8$) and uncoupled ($\mu_c = 0$) conditions. Results are for $\beta = 0$ and $m_2 = 0.018$.

side) and trailing (left-hand side) edges of each contact spots is observed for both cases. Nonetheless, in coupled conditions such a behavior is even heightened.

Let us recall that the indeter slides at constant velocity V. Under this condition any quantity $f(x,t)$ related to the contact problem depends on space and time through the relation $f(x,t) = f(x - Vt)$. So, performing a Fourier transforms leads to $f(q,\omega) = \int dx dt f(x - Vt) e^{-i(qx + \omega t)} = \delta(\omega + qV) f(q)$, and in the case of viscoleastic coatings, Eq. (18) takes the form

$$F_a = \frac{1}{2\pi} \int \frac{\mu_c q^2 \operatorname{Re} \tilde{E}(qV) S_{12}(|q|h) + q|q| \operatorname{Im} \tilde{E}(qV) S_{22}(|q|h)}{S_{22}^2(|q|h) + \mu^2 S_{12}^2(|q|h)} |u_2(q)|^2 dq \qquad (23)$$

where $\tilde{E}(\omega = Vq) = E_0 + i\omega\tau/(1 + i\omega\tau) E_1$ is the complex viscoelastic modulus.

Interestingly, in the case of uncoupled contacts of thin viscoelastic layers (i.e. for $\mu_c = 0$), the friction coefficient $\mu_{a,0}$, arising from the asymmetric contact pressure caused only by viscoelastic hysteresis can be calculated from Eqs. (19,23) as

$$\mu_{a,0} = \frac{1}{2\pi L p_m} \int q|q| \frac{\operatorname{Im} \tilde{E}(qV)}{S_{22}(|q|h)} |u_2(q)|^2 dq$$

Building on the same arguments of Eq. (22), the viscoelastic layer energy balance gives

$$\dot{W} = V\left[\int_\Omega p(x) v_2'(x) dx - \mu_c \int_\Omega p(x) v_1'(x) dx \right] \qquad (24)$$

where $\dot{W}$ is the the contribution to energy dissipation per unit time due to the hysteretic behavior of the viscoelastic material..

Figures 4 show the friction coefficient μ_a due to asymmetric contact pressure for both coupled (i.e. $\mu_c = 0.8$) and uncoupled (i.e. $\mu_c = 0$) conditions as a function of the dimensionless sliding speed ζ for two different values of the dimensionless normal load. As expected, regardless of the coupling, curves follow the well-known bell shaped trend with respect to the sliding velocity (i.e the excitation frequency), although in coupled conditions globally
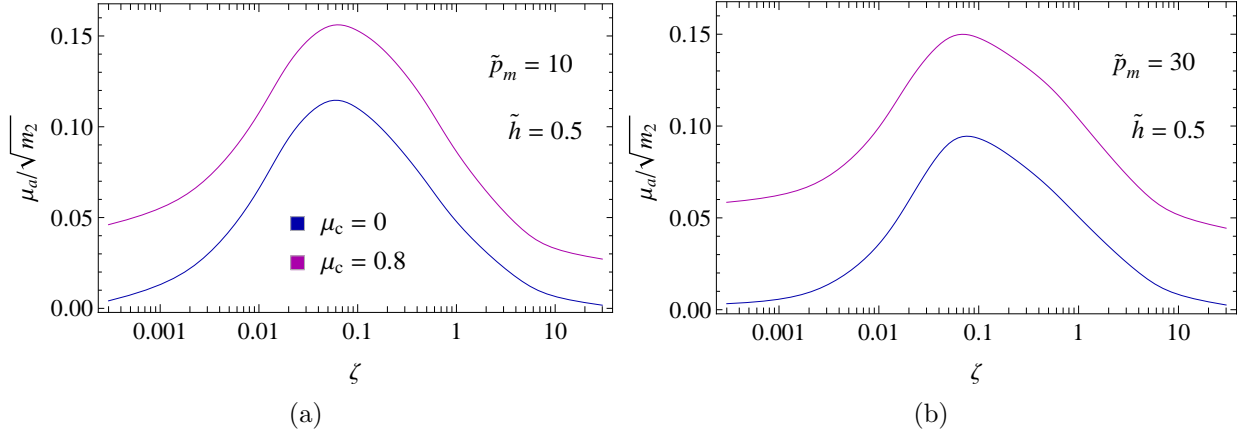
9

FIG. 4: The normalized friction coefficient $\mu_a/\sqrt{m_2}$ for viscoelastic coatings as a function of the dimensionless sliding speed ζ under different normal loads. Results refer to $\beta = 0$ and $m_2 = 0.018$.

higher friction is reported. However, even for $\zeta \to 0$ and $\zeta \to \infty$ where viscoelastic material response is almost elastic and no viscoelastic bulk dissipation occurs, non-vanishing friction is reported due to geometric coupling. Interestingly, the shifting factors between coupled and uncoupled frictional behavior (i.e. the difference between the pink and blue curves) depends on the excitation frequency, resulting higher at lower sliding velocity. Furthermore, comparing Figures 4a-4b, we observe that μ_a in coupled contacts appears less sensitive to the normal load variation compared to uncoupled contact conditions.
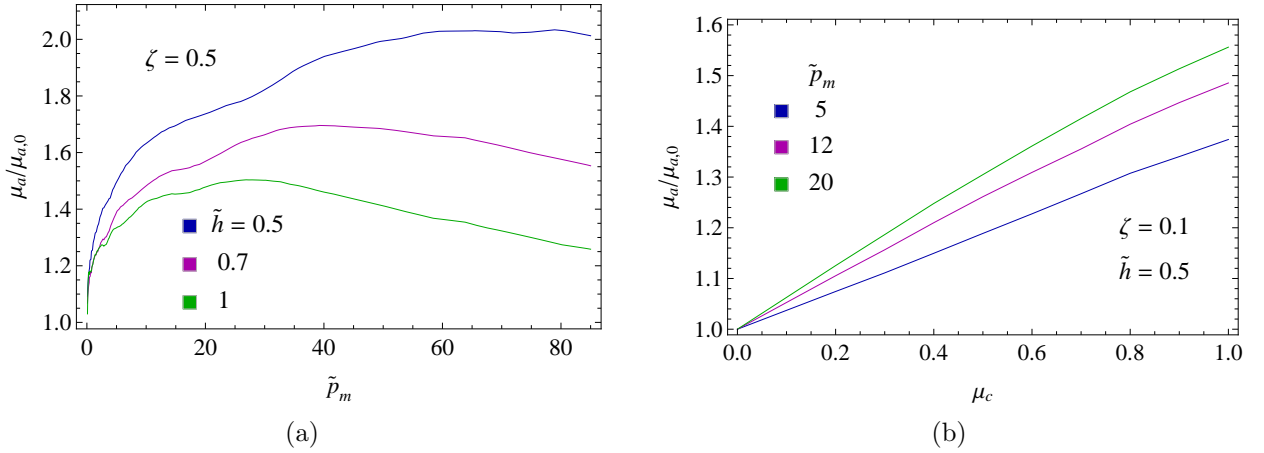

FIG. 5: The friction ratio $\mu_a/\mu_{a,0}$ between the coupled and uncoupled viscoelastic friction coefficients as a function of: (a) the dimensionless contact mean pressure $\tilde{p}_m/\sqrt{m_2}$, for different dimensionless coating thickness $\tilde{h}$; (b) the Coulomb friction coefficient μ_c, for different values of $\tilde{p}_m/\sqrt{m_2}$. Results are given for $\beta = 0$ and $m_2 = 0.018$.

In Figures 5 we report results in terms of the friction ratio $\mu_a/\mu_{a,0}$. Specifically, in Fig.

5a, the effect of $\tilde{p}_m$ is investigated for three different values of $\tilde{h}$. Of course, according to Eqs. (7-11) thinner coatings lead to higher degrees of *geometric* coupling. In Fig. 5b the effect of the Coulomb friction coefficient μ_c is explored at relatively low contact mean pressures. As already discussed for elastic contacts, increasing μ_c exacerbates the effects of the normal-tangential coupling, thus leading to larger values of μ_a. Nonetheless, depending on the specific value of the normal load, a saturation of the phenomenon is also expected.
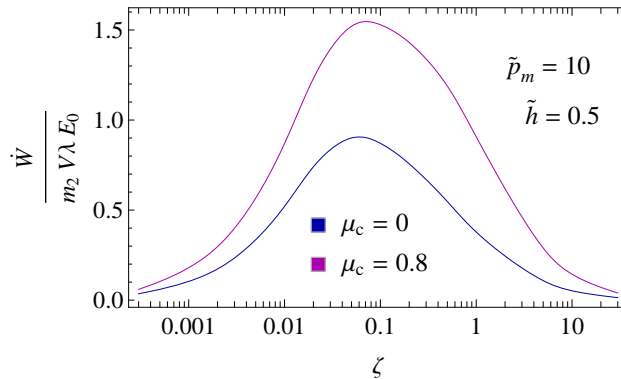
FIG. 6: The dimensionless bulk energy dissipation $\dot{W}/(m_2 V \lambda E_0)$ in viscoelastic thin coatings as a function of the dimensionless sliding speed ζ. Results are given for $\beta = 0$ and $m_2 = 0.018$.

Figure 6 investigates the bulk energy dissipation in viscoelastic coatings. In coupled conditions (i.e. $\mu_c \neq 0$) increased bulk energy dissipation is observed as, from Eq. (24) also the tangential deformations can contribute to the viscoelastic dissipation, depending on the sign of the second right-hand integral. Interestingly, since the energy dissipated is converted into bulk heat, such a peculiar behavior of viscoelastic thin layers in the presence of interfacial friction may be relevant when aiming at controlling the material warming. It is the case, for instance, of tyres in which a key component is the tread (a thin coating on the underlaying stiffer tyre structure) whose warming is crucial for the overall system performance. Neglecting the effect of geometric coupling due to the layer thickness in such systems may significantly alter the theoretical predictions.

B. Viscoelastic contact behavior

In this section we investigated the rough contact results is terms of mean contact quantities (contact area, mean pressure and mean penetration) and displacement fields. We refer our analysis to the case of thin viscoelastic coatings shown in Figure 1, assuming $\beta = 0$, so that the only source of coupling is related to the layer thickness. Notably, in Ref. [28] a similar investigation has been devoted to the case of elastic thin layers.

1. Mean contact quantities

Figures 7 present the main contact behavior of the viscoelastic thin layer in terms of the main contact quantities. Interestingly, regardless of the physical quantity under inves-
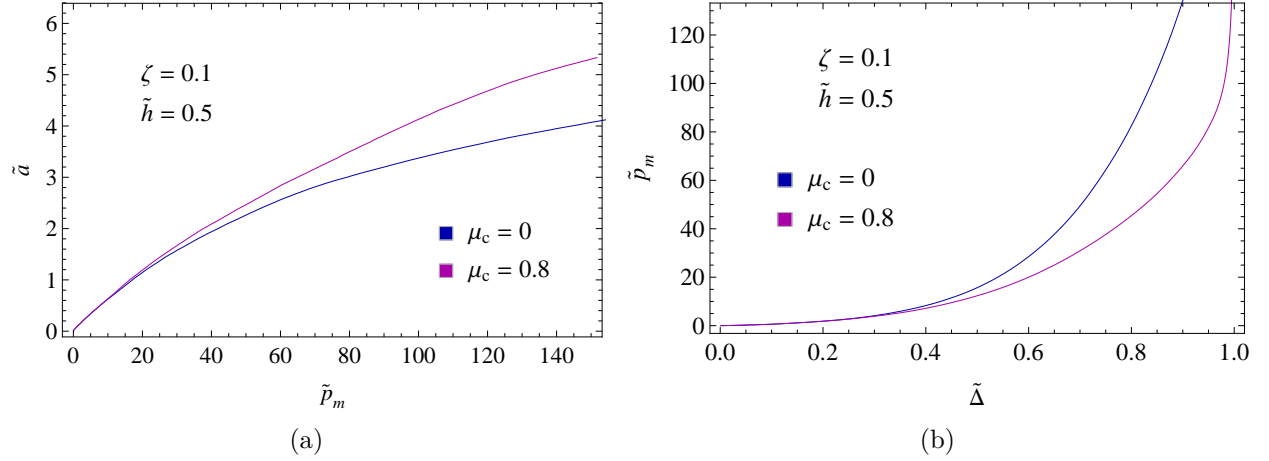
FIG. 7: The dimensionless contact area $\tilde{a}$ as a fucntion of the dimensionless contact mean pressure $\tilde{p}_m$ (a); and the dimensionless contact mean pressure $\tilde{p}_m$ as a function of the dimensionless contact penetration $\tilde{\Delta}$. Full contact is for $\tilde{a} = 2\pi$. Results refer to $\beta = 0$ and $m_2 = 0.018$.

tigation, we note that the difference among the coupled (i.e. $\mu_c \neq 0$) and uncoupled (i.e. $\mu_c = 0$) results increases with $\tilde{p}_m$ increasing. This can be explained, in agreement with Ref. [28], by observing that, from Eq. (1), the shear stresses are proportional to the normal pressure, thus, at low values of $\tilde{p}_m$, even in the case of $\mu_c \neq 0$ low tangential stresses occurs thus leading to a poor normal-tangential coupling. On the contrary, increasing $\tilde{p}_m$ leads to higher shear stresses and, in turn, to larger coupling effects.
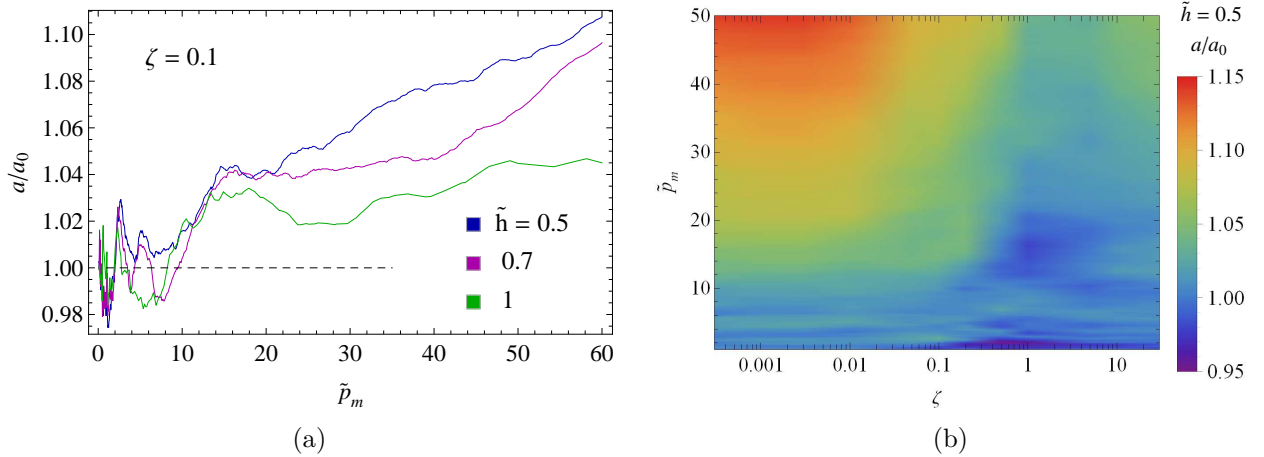

FIG. 8: The contact size ratio a/a_0, between the contact are length associated to coupled ($\mu_c = 0.8$) and uncoupled ($\mu_c = 0$) conditions, as a fucntion of: (a) the dimensionless contact mean pressure $\tilde{p}_m$, for different values of the dimensionless layer thickness $\tilde{h}$; (b) the dimensionless contact mean pressure $\tilde{p}_m$ and the dimensionless sliding speed ζ. Results refer to $\beta = 0$ and $m_2 = 0.018$.

12

Figure 8a shows the contact size ratio a/a_0 as a function of the contact mean pressure $\tilde{p}_m$, for different values of the dimensionless coating thickness $\tilde{h}$, where a represent the contact size in coupled conditions, and a_0 refers to the frictionless uncoupled ones. Notably, the initial results scattering depends on the fact that, at low values of $\tilde{p}_m$, the contact occurs on very small contact spots, mostly localized on top of the roughness crests. This dramatically affects the statistical sampling of the rough profiles, thus leading to noisy results. However, we can still observe that, for $\tilde{p}_m \lesssim 10$, a slight coupling effect is reported on the final contact area size. On the contrary, for $\tilde{p}_m \gtrsim 10$, since the contact size globally increases, frictional shear stress start to play a key role on the contact behavior. Indeed, according to Eqs. (2,6-8), due to *geometric* coupling, the shear stresses also affect the normal displacements of the contacting interfaces, thus leading to a marked increase of the contact area in coupled conditions compared to the frictionless case where no coupling occurs. As expected, increasing the coating thickness flattens the ratio a/a_0 towards the unity value, as with $\beta = 0$ Eqs. (7,11) show that coupling terms monotonically decrease with $\tilde{h}$ increasing, eventually leading, for $\tilde{h} \gtrsim 10$, to the uncoupled half-space contact behavior (see also Ref. [28]).

Figure 8b shows a contour map of the contact size ratio a/a_0, for a specific value of $\tilde{h}$, as a function of both the dimensionless sliding speed ζ and $\tilde{p}_m$. Interestingly, we observe that stronger coupling effects are predicted at low sliding speed, as the ratio a/a_0 at low values of ζ is globally higher than what observed at high values of ζ. However, the trend of a/a_0 vs ζ is non-monotonic, presenting a minimum at $\zeta \approx 1$. The results shown in Fig. 8b offer interesting perspectives, as a contact length increase as high as 15% can be achieved in coupled conditions. Such a large difference suggests that in real life contact problems involving sliding thin viscoelastic layers (e.g. the accurate detection of finger prints on touch screens), the real contact area can be significantly underestimated by neglecting normal-tangential coupling effects. Moreover, according to Eqs. (7,11), the thinner the viscoelastic layer involved, the larger the error in the contact area predicted by uncoupled models.

2. Normal displacement field

A detailed comparison of the normal displacement fields reported in Figure 3 reveals that coupled and uncoupled contacts presents macroscopic differences in the deformed shape of the viscoelastic layer. However, the close-up shown in the same Figure suggests that most of the differences actually occur to the larger spatial scales, as the behavior at the smaller scales appears much more similar among the two cases

In this regard, Figure 9a offers a quantitative comparison between the Power Spectral Density (PSD) $C(q)$ of the deformed profiles under coupled (i.e. $\mu_c \neq 0$) and uncoupled (i.e. $\mu_c = 0$) conditions, under load controlled conditions. The rigid rough profile PSD is also shown (black curve) to help the comparison. Results indicate that in the presence of geometric coupling enhanced large scale deformations occur (i.e. at lower spatial frequencies q) compared to uncoupled case. Such a result is even more clearly shown in Fig. 9b, where we plot the ratio C_{cp}/C_{uncp} between the deformed profile PSD C_{cp} under coupled and C_{uncp} uncoupled conditions. According to Eqs. (7,11), the coupling effect on each deformation scale $\lambda_i = 2\pi/q$ increases with qh reducing, thus leading to larger difference between coupled and uncoupled response at the larger scales. On the contrary, at smaller
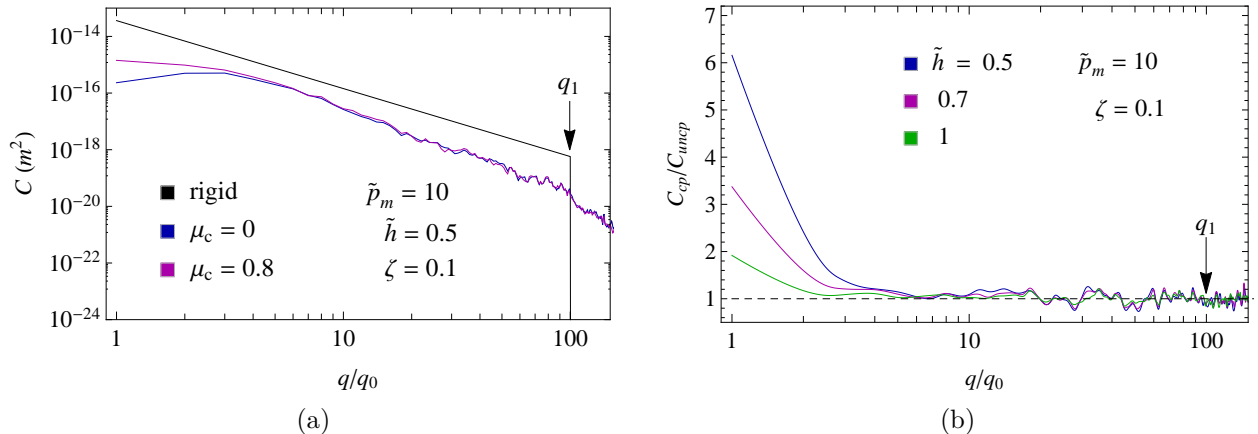
13

FIG. 9: (a) the PSD C of the normal displacement fields for both the coupled and uncoupled conditions as a function of the dimensionless spatial frequency q/q_0; the ratio C_{cp}/C_{uncp} of the mormal displacement PSD under coupled and uncoupled conditions as a function of the dimensionless spatial frequency q/q_0, for different coating dimensionless thickness $\tilde{h}$. Coupled conditions refer to $\mu_c = 0.8$, whereas the uncoupled case is for $\mu_c = 0$. Results refer to $\beta = 0$ and $m_2 = 0.018$.

scales (i.e. for $\lambda_i = 2\pi/q \ll h$) the contact behavior recovers the one expected in the case of half-space contacts, as the normal-tangential coupling terms of Eqs. (7,11) vanish. Building on dimensional arguments, we expect that for $q/q_0 > \rho/\tilde{h}$ the coupling effect should vanish (with ρ being a constant of order unity), as indeed reported in Fig. 9b where we observe that the spatial frequency q at which the coupling effects vanish (i.e. $C_{cp}/C_{uncp} \approx 1$) increases with $\tilde{h}$ decreasing.

The effect of the *geometric* coupling on the spectrum of the viscoelastic normal displacement field can be further explored by defining θ as the ratio between the mean square roughness of the deformed profile and the rigid one, i.e.

$$\theta = \frac{\int_{q_0}^{q_1} C(q)\, dq}{\int_{q_0}^{q_1} C_r(q)\, dq} = \frac{\langle u_2^2 \rangle}{\langle r^2 \rangle} \tag{25}$$

where $\langle u_2^2 \rangle$ and $\langle r^2 \rangle = r_{rms}^2$ are the mean square roughness of the deformed profile and the rigid indenter, respectively.

In Figure 10a we show θ as a function of the contact area fraction a/λ (notably, λ is the full contact area value) for both the coupled contact condition and the uncoupled one. Of course, in both cases, for $a/\lambda \to 1$ the value of θ tends to unity as, regardless of the degree of coupling, the coating displacements completely match the rigid rough profile. However, for $a/\lambda < 1$, higher values of θ are reported in coupled conditions, thus indicating that in the presence of coupling (i.e. for $\mu_c \neq 0$) the deformed interface is globally closer to the rigid counterpart than in uncoupled conditions. Although the contact spots can be differently located in each case, the comparison of Fig. 10a is performed at given total contact length thus the difference in θ has to be mostly ascribed to the non-contact region, where the displacements of the deformable coating in coupled conditions present thinner gaps to the
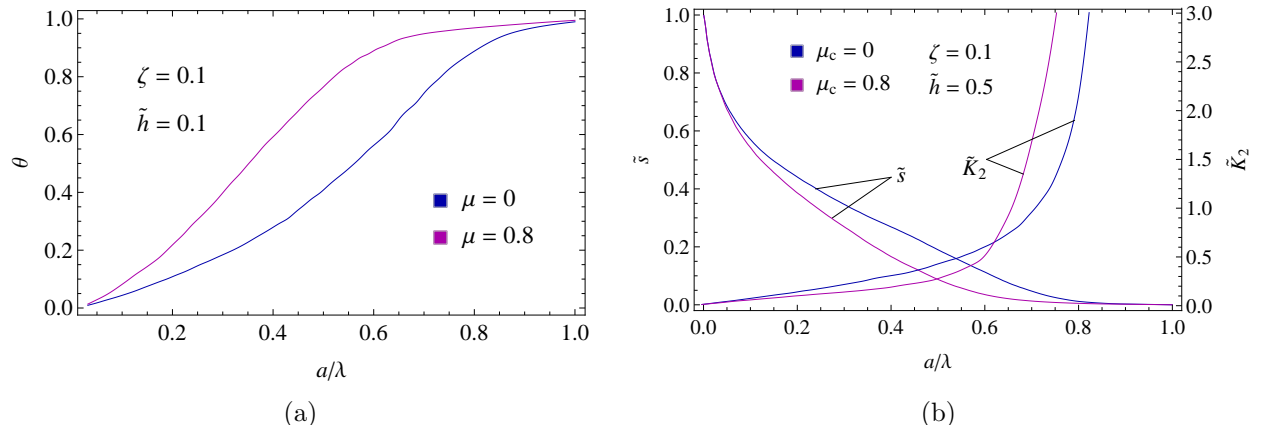
14

FIG. 10: The ratio θ between the frictional coupled and frictionless uncoupled systems mean square heights of the deformed profiles (a), and the dimensionless contact mean separation $\tilde{s} = s/\Lambda$ and the dimensionless normal stiffness $\tilde{K}_2 = 10^{-3} d\tilde{p}_m/d\tilde{\Delta}$ as a function of the contact area fraction a/λ. For the frictional coupled case, the friction coefficient is $\mu_c = 0.8$.

rigid profile compared to the uncoupled case. This can be further investigated by looking at the contact mean separation

$$s = \frac{1}{\lambda} \int_\lambda g(x)\, dx = \Lambda - \Delta$$

where $g(x) = r(x) - [u(x) + \Delta - \Lambda]$ is the gap function between the deformed viscoelastic surface and the rigid profile (notably, $g(x) = 0$ for $x \in \Omega$). Indeed, in Fig. 10b we plot the dimensionless normal separation $\tilde{s}$ against a/λ, showing that thinner gaps are expected in the case of frictional coupled contacts compared to the frictionless uncoupled case. In the same figure, also the contact stiffness $K_2 = dp_m/d\Delta$ is shown indicating that the additional normal deformation introduced by the coupling term G_{21} in Eq. (2) leads to different results, depending on the contact area size. Indeed, for the case under investigation, for a contact area length up to 60% of the full contact length λ (i.e. in most of the practical applications) the frictional coupled case present lower contact stiffness compared to the frictionless uncoupled one. Only at very large contact area the scenario is reversed.

IV. CONCLUSIONS

In this work we have investigated the frictional behavior of thin coatings bonded to rigid substrates in sliding rough contact. The analysis aims at exploring the effect of the peculiar coupling between the normal and tangential displacement fields arising in the case of thin bodies, even for similar contacting materials. The presence of Coulomb friction interactions, through non-null interfacial tangential stresses, activate the coupling effects, which instead vanishes in frictionless contacts.

We found that, in the presence of sufficiently thin layers, normal-tangential coupling occurs so that even in purely elastic rough contacts, where no bulk dissipation occurs, asymmetric contact pressure distributions are reported during sliding, thus resulting in a tangential force opposing the motion larger than that resulting from Coulomb friction considered in isolation. The friction force increase is governed by the mean square slope of the rough counterpart, resulting non-negligible in the range of slope values typical of real surfaces. A similar behavior is observed also in the case of thin viscoelastic layers, where in the presence of interfacial Coulomb friction normal-tangential coupling occurs and higher viscoelastic friction is achieved compared to the uncoupled case, this time also associated to higher bulk energy dissipation. As a consequence, since in real contacts of thin viscoelastic layers interfacial friction is more likely to occur, higher overall friction and faster bulk warming can be expected, with non-negligible effect on the tribological behavior of the interface (e.g. tyre frictional performance).

Results show that the *geometric* coupling between normal-tangential fields enhances the normal displacements on large scales. This, under given normal load, corresponds to significantly larger contact areas size in coupled conditions compared to uncoupled systems, and a resulting lower normal stiffness of the contact interface.

This study proves that, in contacts involving thin deformable coatings bonded to significantly stiffer substrates, neglecting the effect of cross-coupled interfacial shear stresses may lead to significant underestimation of the overall friction and contact area.

Appendix A: Effect of dissimilar materials in thin elastic layers contacts

The case of dissimilar elastic contacting materials can be investigated by assuming the Dundurs' second constant $\beta \neq 0$ [32, 33]. Since, for simplicity, here we focus on the contact between a deformable solid and a rigid one, it takes the form $\beta = (1 - 2\nu)/2(1 - \nu) \neq 0$. Under these conditions, for thin elastic layers in sliding frictional contacts, both the *material* (i.e. the first right-hand side term, vanishing for $\beta = 0$) and *geometric* coupling (i.e. the first right-hand side term) terms in Eq. (7) are non-vanishing, thus resulting in asymmetric contact pressure distribution. Interestingly, the two terms have opposite effects on the normal displacements so that, through Eqs. (18,20), the former term is expected to reduce the friction force, whereas the latter term leads to globally higher friction force. Moreover, according to Ref. [28], dimensional arguments suggest that the correlation length of the *geometric* term (of order unity of h) is larger than that associated to the *material* one.

Figures 2 show the friction coefficient μ_a resulting from asymmetric contact pressure in the case of elastic contacts, for different values of β. Specifically, in Figure 11a μ_a is shown against $\tilde{p}_m$. For $\beta = 0.28$ (i.e. for $\nu = 0.3$), at very low contact pressure, since
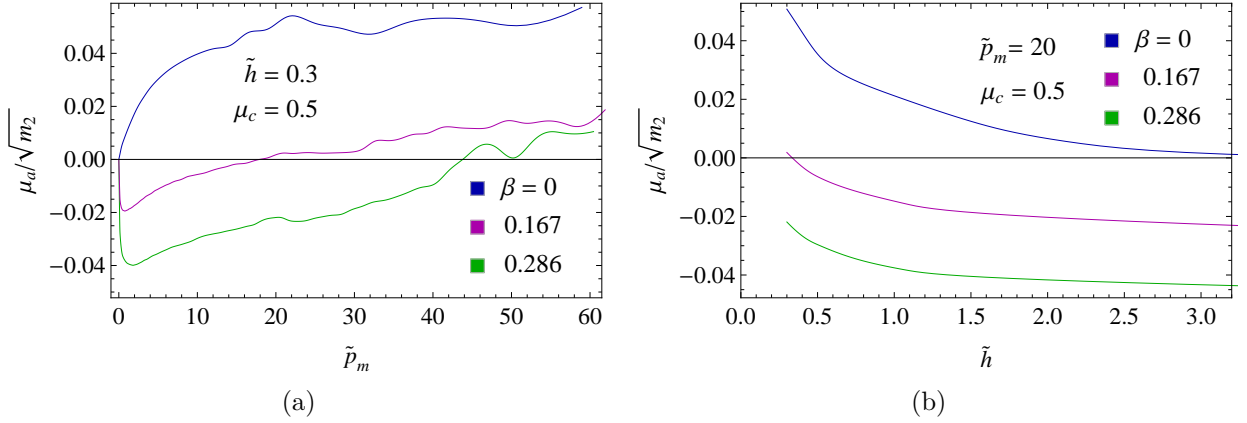
FIG. 11: The friction coefficient μ_a due to asymmetric contact pressure distribution as a function of (a) the dimensionless contact mean pressure $\tilde{p}_m$ and (b) the elastic layer dimensionless thickness $\tilde{h}$. Results results refers to $m_2 = 0.018$.

the contact spots are sufficiently small, the material coupling effect is enhanced due to its shorter correlation length, thus leading to a reduction of the total friction force F_t opposing the relative layer-indenter motion (see Eq. (20)). However, as the normal load increases, larger contact spots are experienced and the *geometric* coupling starts playing a key role, thus increasing μ_a. For sufficiently large values of $\tilde{p}_m$, the geometric coupling term is dominant, thus $\mu_a > 0$ and overall increase of the total friction is expected compared to the uncoupled case (i.e. $\mu_c = 0$). Furthermore, figure 11b shows the effect of the elastic coating thickness on μ_a. Of course, only the *geometric* term is affected by h, thus curved with $\beta = 0$ and $\beta \neq 0$ are shifted by a quantity which can be roughly estimated as proportional to the *material* term. Notably, for $h \to 0$ in both cases we expect $\mu_a \to 0$, as $u(q) \to 0$ in the second of Eqs. (21).

[1] Dahotre, N. B., & Nayak, S. (2005). Nanocoatings for engine application. Surface and Coatings Technology, 194(1), 58-67.

[2] Kano, M. (2006). Super low friction of DLC applied to engine cam follower lubricated with ester-containing oil. Tribology International, 39(12), 1682-1685.

[3] Voigt, D., Karguth, A., & Gorb, S. (2012). Shoe soles for the gripping robot: Searching for polymer-based materials maximising friction. Robotics and Autonomous Systems, 60(8), 1046-1055.

[4] Greenwood, J. A., & Williamson, J. P. (1966). Contact of nominally flat surfaces. Proc. R. Soc. Lond. A, 295(1442), 300-319.

[5] Bush, A.W., Gibson, R.D., Thomas, T.R., TheElastic Contact of a Rough Surface, Wear 1975;35:87-111.

[6] Persson B.N.J.,Theory of rubber friction and contact mechanics, Journal of Chemical Physics 2001;115:3840 -3861.

[7] Yang, C. and Persson, B.N.J., Molecular Dynamics Study of Contact Mechanics: Contact

Area and Interfacial Separation from Small to Full Contact, Phis, Rev. Lett. 2008;100.

[8] Menga, N., Putignano, C., Carbone, G., & Demelio, G. P. (2014). The sliding contact of a rigid wavy surface with a viscoelastic half-space. Proc. R. Soc. A, 470(2169), 20140392.

[9] Menga, N., Carbone, G., & Dini, D. Do uniform tangential interfacial stresses enhance adhesion? Journal of the Mechanics and Physics of Solids 2018;112:145-156.

[10] Menga, N., Carbone, G., & Dini, D. (2019). Corrigendum to:"Do uniform tangential interfacial stresses enhance adhesion?". Journal of the Mechanics and Physics of Solids 2019;133:103744. Doi: https://doi.org/10.1016/j.jmps.2019.103744

[11] Menga, N., & Carbone, G. (2019). The surface displacements of an elastic half-space subjected to uniform tangential tractions applied on a circular area. European Journal of Mechanics-A/Solids, 73, 137-143.

[12] Hyun, S., Pei, L., Molinari, J.-F., Robbins, M.O., Finite-element analysis of contact between elastic self-affine surfaces, Phys. Rev. E 2004;70.

[13] Campana C., Mueser M.H. and Robbins M.O., Elastic contact between self-affine surfaces: comparison of numerical stress and contact correlation functions with analytic predictions. J. Phys. Condens. Matter 2008;20(35).

[14] Pastewka, L., & Robbins, M. O. Contact area of rough spheres: Large scale simulations and simple scaling laws. Applied Physics Letters 2016;108(22):221601.

[15] Medina S. and Dini D., A numerical model for the deterministic analysis of adhesive rough contacts down to the nano-scale. International Journal of Solids and Structures 2014;51(14):2620-2632.

[16] Müser, M. H., Dapp, W. B., Bugnicourt, R., Sainsot, P., Lesaffre, N., Lubrecht, T. A., ... & Rohde, S. (2017). Meeting the contact-mechanics challenge. Tribology Letters, 65(4), 118.

[17] Menga, N., Afferrante, L., Pugno, N. M., & Carbone, G. (2018). The multiple V-shaped double peeling of elastic thin films from elastic soft substrates. Journal of the Mechanics and Physics of Solids, 113, 56-64.

[18] Homola, A. M., Israelachvili, J. N., McGuiggan, P. M., & Gee, M. L. (1990). Fundamental experimental studies in tribology: the transition from "interfacial" friction of undamaged molecularly smooth surfaces to "normal" friction with wear. Wear, 136(1), 65-83.

[19] Chateauminois, A., & Fretigny, C. (2008). Local friction at a sliding interface between an elastomer and a rigid spherical probe. The European Physical Journal E: Soft Matter and Biological Physics, 27(2), 221-227.

[20] Krick, B. A., Vail, J. R., Persson, B. N., & Sawyer, W. G. (2012). Optical in situ micro tribometer for analysis of real contact area for contact mechanics, adhesion, and sliding experiments. Tribology Letters, 45(1), 185-194.

[21] Ben-David, O., Cohen, G., & Fineberg, J. (2010). The dynamics of the onset of frictional slip. Science, 330(6001), 211-214.

[22] Carbone, G., & Mangialardi, L. (2008). Analysis of the adhesive contact of confined layers by using a Green's function approach. Journal of the Mechanics and Physics of Solids, 56(2), 684-706.

[23] Putignano, C., Carbone, G., & Dini, D. (2015). Mechanics of rough contacts in elastic and viscoelastic thin layers. International Journal of Solids and Structures, 69, 507-517.

[24] Menga, N., L. Afferrante, and G. Carbone. Adhesive and adhesiveless contact mechanics of elastic layers on slightly wavy rigid substrates. International Journal of Solids and Structures 2016;88:101-109.

[25] Menga, N., Afferrante, L. and Carbone, G., Effect of thickness and boundary conditions on

the behavior of viscoelastic layers in sliding contact with wavy profiles, The Journal of the Mechanics and Physics of Solids 2016;95: 517-529.

[26] Menga, N., Foti, D., & Carbone, G. Viscoelastic frictional properties of rubber-layer roller bearings (RLRB) seismic isolators. Meccanica 2017;52(11-12):2807-2817.

[27] Menga, N., Dini, D., & Carbone, G. (2020). Tuning the periodic V-peeling behavior of elastic tapes applied to thin compliant substrates. International Journal of Mechanical Sciences, 170, 105331.

[28] Menga, N. (2019). Rough frictional contact of elastic thin layers: The effect of geometric coupling. International Journal of Solids and Structures, 164, 212-220.

[29] Bentall, R. H., & Johnson, K. L. (1968). An elastic strip in plane rolling contact. International Journal of Mechanical Sciences, 10(8), 637-663.

[30] Nowell, D., & Hills, D. A. (1988). Contact problems incorporating elastic layers. International Journal of Solids and Structures, 24(1), 105-115.

[31] Nowell, D., and D. A. Hills. "Tractive rolling of tyred cylinders." International journal of mechanical sciences 30.12 (1988): 945-957.

[32] Sackfield, A., Hills, D. A., & Nowell, D. (2013). Mechanics of elastic contacts. Elsevier.

[33] Barber, J. R. (2018). Contact mechanics (Vol. 250). Springer.

[34] Nowell, D., Hills, D. A., & Sackfield, A. (1988). Contact of dissimilar elastic cylinders under normal and tangential loading. Journal of the Mechanics and Physics of Solids, 36(1), 59-75.

[35] Chen, W. W., & Wang, Q. J. (2008). A numerical model for the point contact of dissimilar materials considering tangential tractions. Mechanics of Materials, 40(11), 936-948.

[36] Chen, W. W., & Wang, Q. J. (2009). A numerical static friction model for spherical contacts of rough surfaces, influence of load, material, and roughness. Journal of Tribology, 131(2), 021402.

[37] Wang, Z. J., Wang, W. Z., Wang, H., Zhu, D., & Hu, Y. Z. (2010). Partial slip contact analysis on three-dimensional elastic layered half space. Journal of Tribology, 132(2), 021403.

[38] Elloumi, R., Kallel-Kamoun, I., & El-Borgi, S. (2010). A fully coupled partial slip contact problem in a graded half-plane. Mechanics of Materials, 42(4), 417-428.

[39] Jaffar, M. J. (1993). Determination of surface deformation of a bonded elastic layer indented by a rigid cylinder using the Chebyshev series method. Wear, 170(2), 291-294.

[40] Jaffar, M. J. (1997). A numerical investigation of the sinusoidal model for elastic layers in line contact. International journal of mechanical sciences, 39(5), 497-506.

[41] Kogut, L., & Komvopoulos, K. (2003). Electrical contact resistance theory for conductive rough surfaces. Journal of Applied Physics, 94(5), 3153-3162.

[42] Menga, Nicola, and Michele Ciavarella. "A Winkler solution for the axisymmetric Hertzian contact problem with wear and finite element method comparison." The Journal of Strain Analysis for Engineering Design 50.3 (2015): 156-162.

[43] Carbone, G., & Mangialardi, L. (2008). Analysis of the adhesive contact of confined layers by using a Green's function approach. Journal of the Mechanics and Physics of Solids, 56(2), 684-706.

[44] Menga, N., Afferrante, L., Demelio, G. P., & Carbone, G. Rough contact of sliding viscoelastic layers: numerical calculations and theoretical predictions. Tribology International, 2018; 122:67-75.

[45] Maugis, D., Contact Adhesion and Rupture of Elastic Solids. Springer-Verlag Berlin Heidelberg, 2000.

[46] Christensen, R., (1982). Theory of Viscoelasticity. Academic Press

[47] Persson, B. N., Albohr, O., Tartaglino, U., Volokitin, A. I., & Tosatti, E. (2004). On the nature of surface roughness with application to contact mechanics, sealing, rubber friction and adhesion. Journal of physics: Condensed matter, 17(1), R1.

[48] Lorenz, B., Persson, B. N. J., Fortunato, G., Giustiniano, M., & Baldoni, F. (2013). Rubber friction for tire tread compound on road surfaces. Journal of Physics: Condensed Matter, 25(9), 095007.